Available online at www.sciencedirect.com

ScienceDirect

International Journal of Solids and Structures 44 (2007) 672–684

INTERNATIONAL JOURNAL OF SOLIDS and STRUCTURES

www.elsevier.com/locate/ijsolstr

Modeling of wireless remote shape control for beams using nonlinear photostrictive actuators

Dongchang Sun, Liyong Tong *

School of Aerospace, Mechanical and Mechatronic Engineering, The University of Sydney, NSW 2006, Australia

Received 21 July 2005; received in revised form 3 May 2006
Available online 11 May 2006

Abstract

Photostrictive materials produce mechanical strain when irradiated by ultraviolet light, thus may be used in wireless remote control of smart microstructures. This paper presents an investigation into modelling and static shape control of beams with nonlinear photostrictive actuators. Governing equations of beams bonded with photostrictive actuator patches are derived to study the interaction between the photostrictive actuators and the host beams. An analytical solution method is presented to solve the governing equations of the beams with discretely distributed photostrictive actuators. An iterative procedure is developed to find optimal light intensities in photostrictive actuators that best match the actuated shape to the desired one. An example is given to illustrate the model and shape control of a beam with PLZT actuators.

Keywords: Photostrictive actuators; Static shape control; Piezoelectric transducers; Wireless remote control; Smart structures

1. Introduction

Photostrictive materials have potential applications in wireless remote control of smart microstructures due to their ability of converting photonic energy to mechanical energy. The mechanism of photostrictive effect can be described as the combination of the photovoltaic and converse piezoelectric effects (Fridkin, 1979). When the photostrictive materials are illuminated by light of certain wavelength, a high voltage considerably exceeding the energy gap is generated (Poosanaas et al., 2000). Due to the converse piezoelectric effect, mechanical strain is then induced by this photovoltage. Use of photostrictive materials as actuators creates an opportunity for developing wireless remotely controlled micromachines with high mobility that remove the need to integrate all complex and bulky components, such as power, light generator, control device and remote sensing systems, on board.

Research on photostrictive materials has been a focus in physics and material science in recent years. Current research in this field is mainly on the enhancement of the photostrictive effect of materials by controlling and optimizing processing parameters, ceramic composition and dopant type/content (Nonaka et al., 1998;

* Corresponding author. Tel.: +61 2 9351 6969; Fax: +61 2 9351 4841.
E-mail address: Ltong@aeromech.usyd.edu.au (L. Tong).

0020-7683/$ - see front matter
doi:10.1016/j.ijsolstr.2006.05.013

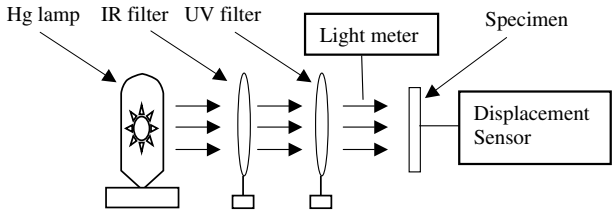

Fig. 1. Typical experiment setup for measuring strains of photostrictive materials induced by light irradiation.

Goldring et al., 2003; Zhou et al., 2004). The photostrictive effect has been found in several materials such piezoelectric ZNS (Fridkin et al., 1984), piezoelectric BI12GEO20 (Fridkin et al., 1987) Lanthanum-modified lead zirconate titanate (PLZT) (Lin et al., 1994), piezoelectric crystal La3Ga5SiO14:Pr (Dalba et al., 1996) and Sn2P2S6 ferroelectric crystal/ceramics (Cho et al., 2001). Among them, PLZT ceramic is one of the most promising photostrictive materials due to its relatively high photostriction and ease of fabrication. The strain of this kind of materials induced by light is about a half of the strain level induced by electric field in widely used piezoelectric materials.

Research has shown that PLZT is sensitive to the near ultraviolet light with a central wavelength of 365 nm. Hg lamps and wavelength filters can be used to produce the desired light beams (Poosanaas et al., 2000). The light generated by Hg lamps passes through infrared (IR) blocking filters and ultraviolet (UV) bandpass filters to produce a monochromatic beam with a maximum strength around 365 nm wavelength. A typical test setup for measuring the relationship between the light induced strain and light intensity is shown in Fig. 1. Applications of PLZT have been also explored based on experimental investigations. Fukuda et al. (1995) tested the actuating behaviour of a bimorph PLZT element and designed a optical servo system using bimorph PLZT. Uchino (1997) developed a photo-driven relay and a wireless walking device using a bimorph configuration. Morikawa and Nakada (1998) proposed an effective position control method for the bimorph-type optical actuator and validated it by experiments. Belforte et al. (1998) designed and constructed a mechanical micro-actuator that can amplify the movement induced in the PLZT via an ultraviolet lamp. Baglio et al. (2002) introduced an actuation strategy based on a photo-thermo-mechanical energy transformation model and designed an actuator prototype. Kawaguchi et al. (2002) tested the electric property of a PZLT specimen and designed an optical motor made of PLZT.

Research on the application of photostrictive actuator in active structural control is relatively rare. Tzou and Chou (1996) investigated the photostrictive characteristics and photodeformation of distributed photostrictive optical actuators and presented two-dimensional (2D) nonlinear constitutive relations of the photodeformation induced by the photostrictive effect. Liu and Tzou (1998) analyzed detailed photostriction, pyroelectricity, thermoelasticity and photodeformation of 2D opto-electromechanical photostrictive actuators, and designed a servo control system to perform vibration control of a rectangular plate using distributed opto-electromechanical actuators. Adequate theories for wireless remote control of structures with distributed photostrictive materials are yet to be developed, and applications to smart structures with photostrictive actuators are to be further explored.

Although the PLZT's response speed to light irradiation has been improved dramatically by optimizing ceramic composition and dopant type in the last five years, the response of bulk material is not fast enough to be used in vibration control of structures so far (Ichiki et al., 2004). Therefore, the focus of this research will be on the quasi-static or static shape control of structures using photostrictive material. A theoretical model of beams with PLZT actuator patches is developed, and a general solution method is presented to solve the governing equations segment by segment. In the shape control, the light intensities of photostrictive actuator patches are treated as the design variables and optimized to best achieve a given desired shape.

2. Constitutive models of photostrictive materials

Since photostrictive materials are special piezoelectric materials, they have the piezoelectric effect. The unique characteristic of the photostrictive materials differentiating themselves from the usual piezoelectric

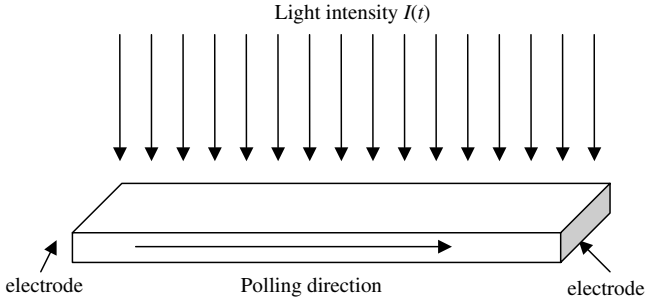

Fig. 2. A photostrictive actuator.

materials is that they also have the photovoltaic effect. The voltage is generated by itself when irradiated by light with specific wavelength rather than being exerted by electric wires. Therefore, the constitutive equations of the photostrictive materials should describe both photovoltaic and piezoelectric effects.

Consider a photostrictive actuator patch shown in Fig. 2. Its left and right surfaces are metallized as two electrodes. When its top surface is irradiated by a uniform ultraviolet light, a current opposite to its polarized direction is generated due to its photovoltaic effect.

The induced current flow charges the electrodes and generates an in-plane electric field $E(t)$. Two models will be given in this section.

2.1. Time dependent model

The electric field induced by a uniform constant transverse illumination can be expressed as (Tzou and Chou, 1996)

$$E(t) = E_s\left[1 - e^{-\frac{I_0 t}{\alpha}}\right] \tag{1}$$

where I_0 denotes the constant intensity of the light illumination, t is the time, and α is a coefficient defined as

$$\alpha = \frac{E_s a_s C_0}{i_0} \tag{2}$$

where E_s is the saturated photovoltaic voltage, a_s is the aspect ratio of length to width, C_0 is the capacitance between two edge electrodes, and i_0 is the short-circuit current per unit illumination intensity due to the photovoltaic effect.

When the light is switched off, the photovoltaic voltage decreases gradually to zero, and this darkness process usually takes more time than that of the illumination process. To include the darkness effect in Eq. (1), we modify Eq. (1) to the following form:

$$E(t) = E_s\left[1 - e^{-\frac{I_0 t}{\alpha + \alpha_d}}\right] \tag{3}$$

where α_d is a constant for the darkness process. For the illumination process, $\alpha_d = 0$.

The photocurrent J_{ph} is directly proportional to the illumination intensity, that is

$$J_{ph} = \alpha_c I_0 \tag{4}$$

where α_c is a constant.

It is showed in Eq. (1) that the photovoltaic voltage gradually attains the saturated photovoltaic voltage after constant illumination intensity is applied. The response speed of the photostrictive material depends on the aspect ratio, the capacitance, the short-circuit current and the illumination intensity. In this model, the maximum photovoltage is constrained by the saturated photovoltaic voltage that is independent of the illumination intensity. This model depicts the time history of the photovoltage for photovoltaic materials.

2.2. DC model

In this model, the photo-induced DC electric field is derived based on the second order optical nonlinearity theory (Uchino, 1997). When considering the second order nonlinear effect, the polarization of dielectrics can be expressed as

$$P = \varepsilon_0(\chi_1 E_{\text{op}} + \chi_2 E_{\text{op}}^2) \tag{5}$$

where ε_0 is a permittivity coefficient of vacuum, χ_1 is the linear susceptibility, χ_2 is the nonlinear susceptibility of the second order, and E_{op} is the electric field at a single optical frequency. Since the light is an electromagnetic wave, it can provide an alternating electric field $E_{\text{op}}\cos\omega_{\text{op}}t$ for charges in dielectrics, in which E_{op} denotes the amplitude and ω_{op} is the optical frequency of the light. In this case, the polarization becomes

$$P = \varepsilon_0(\chi_1 E_{\text{op}}\cos\omega_{\text{op}}t + \chi_2 E_{\text{op}}^2\cos^2\omega_{\text{op}}t) \tag{6}$$

Due to the polarization charges in the polarized dielectrics, an additional field is generated and it should be added to the macroscopic electric field to obtain the local electric field. Using the Lorentz relation (Kittel, 1996), the local field in dielectrics can be approximately expressed by

$$E_{\text{local}} = E + \frac{\gamma P}{3\varepsilon_0} \tag{7}$$

where E is the macroscopic electric field and γ is the Lorentz factor. When an alterative electric field is applied, replacing E with $E_{\text{op}}\cos\omega_{\text{op}}t$ and substituting Eq. (6) into (7), the local field becomes

$$E_{\text{local}} = E_{\text{op}}\cos\omega_{\text{op}}t + \frac{\gamma}{3}(\chi_1 E_{\text{op}}\cos\omega_{\text{op}}t + \chi_2 E_{\text{op}}^2\cos^2\omega_{\text{op}}t) \tag{8}$$

The average value of the local electric field in Eq. (8) is:

$$\overline{E}_{\text{local}} = \frac{1}{6}\gamma\chi_2 E_{\text{op}}^2 \tag{9}$$

Since Eq. (9) is derived under a coherent propagation of the light wave at a single frequency, it should be modified when this condition of coherent illumination is not satisfied in general cases. Therefore, a modified form of Eq. (9) is given by

$$\overline{E}_{\text{local}} = c_1\gamma\chi_2(E_{\text{op}}^2)^{\beta} \tag{10}$$

where c_1 is a constant and $0 < \beta \leqslant 1$ is a parameter of the depression effect which can be determined by experiment. The average induced DC field can be expressed as

$$\overline{E}_{\text{dc}} = \overline{E}_{\text{local}} = c_2\gamma\chi_2 I_{\text{op}}^{\beta} \tag{11}$$

where E_{dc} is the effective DC field induced by the light irradiation, c_2 is a constant and I_{op} is the light intensity.

Based on the photo-induced DC field given in Eq. (11), the photocurrent can be derived as

$$J_{\text{ph}} = c_3 q\mu\gamma\chi_2\frac{I_{\text{op}}^{0.5+\beta}}{\sqrt{R}} \tag{12}$$

where c_3 is a constant, μ is the carrier mobility, q is the charge of the photo-carrier and R is the recombination rate of the carrier.

The strain of the photostrictive material can be expressed as

$$\varepsilon = s\sigma + d_{33}c_2\gamma\chi_2 I_{\text{op}}^{\beta} \tag{13}$$

where ε is the strain, σ is the stress, and d_{33} is the piezoelectric strain constant of the material. The second part on the right hand side of Eq. (13) is the strain induced by the light irradiation. The stress–strain relation of the photostrictive material can also be written in the following form:

$$\sigma = Y\varepsilon - e_{33}c_2\gamma\chi_2 I_{\text{op}}^{\beta} \tag{14}$$

where Y is the Young's modulus, and e_{33} is the piezoelectric stress constant of the material. Denoting $p_{33} = e_{33}c_2\gamma\chi_2$ as the photostrictive stress constant along axis 3, Eq. (14) becomes

$$\sigma = Y\varepsilon - p_{33}I_{\mathrm{op}}^{\beta} \tag{15}$$

Eq. (15) describes the contribution of light intensity to overall stress of the photostrictive materials, and it will be used in shape control of beams in the following sections.

3. Basic equations of photo-actuated beams

3.1. Governing equations

Consider a slender beam bonded with N photostrictive actuator patches on its top surface, as shown in Fig. 3. The length, width and thickness of the host beam are denoted by l, b and h, respectively. However, the material properties of the host beam may be different in different segments. The ith ($i = 1, 2, \ldots, N$) photo-actuator patch has a dimension of $l_i \times b \times h_i$. It is assumed that the photostrictive actuator patches are perfectly bonded. The adhesive layers are assumed to be thin enough so that the transverse shear and peel strains along its thickness can be assumed to be constant. To emphasize the photostrictive effect on the shape control of beams, ventilation in the beam is assumed to be well enough so that the thermo-effect caused by light illumination is negligible. In addition, the effective DC field induced by light irradiation is assumed to be uniform between the two electrodes in each photostrictive actuator.

To perform shape control of a beam, its governing equations should be derived for different segments. There are two types of segments, i.e. the host beam attached with actuators and the host beam itself. We begin with the beam segment bonded with photostrictive actuators. Consider the equilibrium of an infinitesimal portion including the host beam, the ith actuator and the adhesive layer. The equilibrium equations are as follows:

$$T_{\mathrm{a}i,x} + b\tau_i = 0; \quad Q_{\mathrm{a}i,x} + b\sigma_i = 0; \quad M_{\mathrm{a}i,x} + bh_i\tau_i/2 - Q_{\mathrm{a}i} = 0, \ \ i = 1, 2, \ldots, N \tag{16a}$$

$$T_{\mathrm{b}i,x} - b\tau_i = 0; \quad Q_{\mathrm{b}i,x} - b\sigma_i = 0; \quad M_{\mathrm{b}i,x} + bh_{\mathrm{b}}\tau_i/2 - Q_{\mathrm{b}i} = 0 \tag{16b}$$

where the subscripts "a" and "b" represent the actuator layer and the host beam respectively, the subscript x represents the differentiation with respect to x, and u, w are the longitudinal and transverse displacements respectively, h denotes the thickness, τ and σ are the shear and peeling stress of the adhesive layer, T, Q and M are the axial force, transverse shear force and bending moment respectively. τ_i and σ_i are the shear and peal stresses in the thin adhesive layer defined as

$$\tau_i = \frac{Y_{vi}}{2(1+\nu_{vi})h_{vi}}\left[\frac{1}{2}(w_{\mathrm{a}i,x} + w_{\mathrm{b}i,x}) + \frac{1}{2h_{vi}}(h_i w_{\mathrm{a}i,x} + h w_{\mathrm{b}i,x}) + \frac{u_{\mathrm{b}i} - u_{\mathrm{a}i}}{h_{vi}}\right] \tag{17a}$$

$$\sigma_i = \frac{Y_{vi}(1-\nu_{vi})}{(1-2\nu_{vi})(1+\nu_{vi})h_{vi}}(w_{\mathrm{b}} - w_{\mathrm{a}i)} \tag{17b}$$

where h_{vi}, Y_{vi} and ν_{vi} are the thickness, Young's modulus and Poisson's ratio of the ith adhesive layer, respectively.

The strain in x-direction can be expressed as

$$\varepsilon_{\mathrm{a}i} = u_{\mathrm{a}i,x} - z_i w_{\mathrm{a}i,xx} \tag{18}$$

where z_i is the z-coordinate from the neutral plane of the actuator layer. Substituting Eq. (18) into the constitutive relation of the photostrictive actuator in Eq. (15), we have

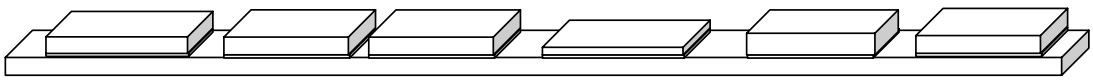

Fig. 3. Beam bonded with photostrictive actuator patches.

$$\sigma_{ai} = Y_{ai}(u_{ai,x} - z_i w_{ai,xx}) - p_{33i} I_i^{\beta} \tag{19}$$

where Y_{ai} is the Young's modulus of the ith actuator, I_i is the light intensity applied on this actuator.

The axial force and the bending moment for the actuator layer can be written as follows:

$$T_{ai} = A_{ai} u_{ai,x} - B_{ai} w_{ai,xx} - b p_{33i} h_i I_i^{\beta}; \quad M_{ai} = B_a u_{ai,x} - D_{ai} w_{ai,xx} - b p_{33i} r_{ai} h_i I_i^{\beta} \tag{20}$$

where r_{ai} is the z-coordinate value of the mid-plane of the actuator layer from the neutral plane of the beam, I_i is the light intensity irradiated on the ith actuator, A_{ai}, B_{ai} and D_{ai} are constants defined as

$$A_{ai} = \int_{z_{li}}^{z_{ui}} b Y_{ai}\,\mathrm{d}z; \quad B_a = \int_{z_{li}}^{z_{ui}} b Y_{ai} z\,\mathrm{d}z; \quad D_{ai} = \int_{z_{li}}^{z_{ui}} b Y_{ai} z^2\,\mathrm{d}z \tag{21}$$

where z_{li} and z_{ui} are the z-coordinates of the lower and upper surfaces of the ith actuator. Eq. (20) shows that the photostrictive effect of the actuator contributes to both axial force resultant and the bending moment, and hence it can be used for active control of the beam.

Denoting

$$T_{ai}^e = T_{ai} + b p_{33i} h_i I_i^{\beta}; \quad M_{ai}^e = M_{ai} + b p_{33i} r_{ai} h_i I_i^{\beta} \tag{22}$$

which represent the axial force and bending moment without the contribution of photostriction of the actuator, and solving the derivatives of the u_{ai} and w_{ai} from Eq. (20), we have

$$u_{ai,x} = \overline{A}_{ai} T_{ai}^e + \overline{B}_{ai} M_{ai}^e; \quad w_{ai,xx}^e = \overline{C}_{ai} T_{ai}^e + \overline{D}_{ai} M_{ai}^e \tag{23}$$

where $\overline{A}_{ai}$, $\overline{B}_{ai}$, $\overline{C}_{ai}$ and $\overline{D}_{ai}$ are constants. Similarly, for the host beam covered by an actuator, we have

$$u_{bi,x} = \overline{A}_{bi} T_{bi}^e + \overline{B}_{bi} M_{bi}^e; \quad w_{bi,xx}^e = \overline{C}_{bi} T_{bi}^e + \overline{D}_{bi} M_{bi}^e \tag{24}$$

where $\overline{A}_{bi}$, $\overline{B}_{bi}$, $\overline{C}_{bi}$ and $\overline{D}_{bi}$ are constants related to the host beam.

It should be noted that T_{ai} and M_{ai} in Eq. (16) can be replaced with T_{ai}^e and M_{ai}^e because the light intensity in each actuator is constant. Introducing the state vectors

$$\mathbf{y}_i = (u_{ai}, T_{ai}, w_{ai}, w_{ai,x}, Q_{ai}, M_{ai}, u_{bi}, T_{bi}, w_{bi}, w_{bi,x}, Q_{bi}, M_{bi})^{\mathrm{T}} \tag{25}$$

and inserting Eq. (17) into Eq. (16), equations in Eq. (16), Eqs. (23) and (24) can be written into the following matrix form:

$$\mathbf{y}_{i,x} = \mathbf{A}_i \mathbf{y}_i, \quad i = 1, 2, \ldots, N \tag{26}$$

where $\mathbf{A}_i \in R^{12\times 12}$ is the coefficient matrix.

The governing equation for the segments without a photostrictive actuator can be obtained by simply dropping out the terms related to the actuator and adhesive layers and takes the form of

$$\mathbf{y}_{hi,x} = \mathbf{A}_{hi} \mathbf{y}_{hi}, \quad i = 1, 2, \ldots, N+1 \tag{27}$$

where $\mathbf{y}_{hi} = (u_{hi}, T_{hi}, w_{hi}, w_{hi,x}, Q_{hi}, M_{hi})^{\mathrm{T}}$ is a six-dimensional state vector and $\mathbf{A}_{hi} \in R^{6\times 6}$ is the coefficient matrix of the host beam.

3.2. Boundary and continuity conditions

For the ith photostrictive actuators, its six boundary conditions at both ends can be expressed in the following general form:

$$\mathbf{D}_{li} \mathbf{y}_i(x_{li}) + \mathbf{D}_{ri} \mathbf{y}_i(x_{ri}) = \mathbf{d}_i \tag{28}$$

where $\mathbf{D}_{li} \in R^{6\times 12}$, $\mathbf{D}_{ri} \in R^{6\times 12}$ are constant matrices, and $\mathbf{d}_i \in R^6$ is a known vector. For example, the boundary conditions of a free-free actuator are $T_{ai} = Q_{ai} = M_{ai} = 0$, i.e. $T_{ai}^e = b p_{33i} h_i I_i^{\beta}$, $Q_{ai} = 0$, $M_{ai}^e = b p_{33i} r_{ai} h_i I_i^{\beta}$. The related boundary matrices and vector are

$$\mathbf{D}_{\mathrm{l}i}=\begin{bmatrix}0&1&0&0&0&0&0&0&0&0&0&0\\0&0&0&0&1&0&0&0&0&0&0&0\\0&0&0&0&0&1&0&0&0&0&0&0\\0&0&0&0&0&0&0&0&0&0&0&0\\0&0&0&0&0&0&0&0&0&0&0&0\\0&0&0&0&0&0&0&0&0&0&0&0\end{bmatrix},$$

$$\mathbf{D}_{\mathrm{r}i}=\begin{bmatrix}0&0&0&0&0&0&0&0&0&0&0&0\\0&0&0&0&0&0&0&0&0&0&0&0\\0&0&0&0&0&0&0&0&0&0&0&0\\0&1&0&0&0&0&0&0&0&0&0&0\\0&0&0&0&1&0&0&0&0&0&0&0\\0&0&0&0&0&1&0&0&0&0&0&0\end{bmatrix},\quad \mathbf{d}_i=\begin{pmatrix}1\\0\\r_{\mathrm{a}i}\\1\\0\\r_{\mathrm{a}i}\end{pmatrix} bp_{33i}h_iI_i^{\beta} \tag{29}$$

Similarly, the boundary conditions for the host beam can be expressed as

$$\mathbf{D}_{\mathrm{l}}\mathbf{y}_{\mathrm{h}1}(0)+\mathbf{D}_{\mathrm{r}}\mathbf{y}_{\mathrm{h}N+1}(l)=\mathbf{d}_{\mathrm{h}} \tag{30}$$

The continuity at the interfaces between the actuator covered segments and the host beam should be imposed to ensure continuity of the displacements and equilibrium of forces in the host beam. The continuity conditions at the ends of the ith photostrictive actuator path can be expressed by

$$\mathbf{y}_{\mathrm{h}i}(x_{\mathrm{l}i})=\mathbf{G}\mathbf{y}_i(x_{\mathrm{l}i}),\quad \mathbf{y}_{\mathrm{h}i}(x_{\mathrm{r}i})=\mathbf{G}\mathbf{y}_i(x_{\mathrm{r}i}),\quad i=1,2,\ldots,N \tag{31}$$

where $\mathbf{G}=\lfloor \mathbf{0}_{6\times 6}\quad \mathbf{I}_{6\times 6}\rfloor$ is a transformation matrix, $\mathbf{I}_{6\times 6}$ represents a 6×6 identity matrix.

The governing equations in Eqs. (26) and (27) together with the boundary and continuity conditions in Eqs. (28), (30) and (31) form the theoretical foundation for the wireless remote shape control using photostrictive actuators.

3.3. Solutions

By solving the differential equations in Eq. (26), the displacements and generalized forces of the ith actuator covered segment at any point x can be obtained as

$$\mathbf{y}_i(x)=\mathbf{\Phi}_i(x)\mathbf{y}_i(x_{\mathrm{l}i})\quad x_{\mathrm{l}i}<x\leqslant x_{\mathrm{r}i},\quad i=1,2,\ldots,N \tag{32}$$

where $\mathbf{\Phi}_i(x)=\exp[\mathbf{A}_i(x-x_{\mathrm{l}i})]$ is a 12×12 transition matrix for the composite segment. By solving Eq. (27) for the host beam segments, we have

$$\mathbf{y}_{\mathrm{h}i}(x)=\mathbf{\Phi}_{\mathrm{h}i}(x)\mathbf{y}_{\mathrm{h}i}(x_{\mathrm{r}i-1}),\quad x_{\mathrm{r}i-1}<x\leqslant x_{\mathrm{l}i}(x_{\mathrm{r}0}=0,x_{\mathrm{l}N+1}=l),\quad i=1,2,\ldots,N+1 \tag{33}$$

where $\mathbf{\Phi}_{\mathrm{h}i}(x)=\exp[\mathbf{A}_{\mathrm{h}i}(x-x_{\mathrm{r}i-1})]$ is the transition matrix for the host beam segment.

If the state vectors $\mathbf{y}_{\mathrm{h}i}$ and $\mathbf{y}_i$ at all interface points $x_{\mathrm{l}i}$ and $x_{\mathrm{r}i}$ $(i=1,2,\ldots,N)$ are determined, the responses of the beam to the light irradiation at all segments can be obtained from Eqs. (32) and (33). These state vectors at interfaces can be obtained by solving the following algebraic equations:

$$\begin{aligned}
&\mathbf{y}_{\mathrm{h}i}(x_{\mathrm{l}i})=\mathbf{\Phi}_{\mathrm{h}i}(x_{\mathrm{l}i})\mathbf{y}_{\mathrm{h}i}(x_{\mathrm{r}i-1}),\quad i=1,2,\ldots,N+1\\
&\mathbf{y}_i(x_{\mathrm{r}i})=\mathbf{\Phi}_i(x_{\mathrm{r}i})\mathbf{y}_i(x_{\mathrm{l}i}),\quad i=1,2,\ldots,N\\
&\mathbf{y}_{\mathrm{h}i}(x_{\mathrm{l}i})=\mathbf{G}\mathbf{y}_i(x_{\mathrm{l}i}),\mathbf{y}_{\mathrm{h}i}(x_{\mathrm{r}i})=\mathbf{G}\mathbf{y}_i(x_{\mathrm{r}i}),\quad i=1,2,\ldots,N\\
&\mathbf{D}_{\mathrm{l}i}\mathbf{y}_i(x_{\mathrm{l}i})+\mathbf{D}_{\mathrm{r}i}\mathbf{y}_i(x_{\mathrm{r}i})=\mathbf{d}_i,\quad i=1,2,\ldots,N\\
&\mathbf{D}_{\mathrm{l}}\mathbf{y}_{\mathrm{h}1}(0)+\mathbf{D}_{\mathrm{r}}\mathbf{y}_{\mathrm{h}N+1}(l)=\mathbf{d}_{\mathrm{h}}
\end{aligned} \tag{34}$$

There are $36N+12$ equations and $36N+12$ unknown state variables in Eq. (34). Equations in (34) can be rewritten in the following matrix form:

$$\overline{\mathbf{\Phi}}\bar{\mathbf{y}} = \overline{\mathbf{d}} \tag{35}$$

where

$$\overline{\mathbf{\Phi}} = \begin{bmatrix}
\mathbf{\Phi}_{\mathrm{h}1}(x_{\mathrm{l}1}) & -\mathbf{I}_6 & 0 & 0 & 0 & 0 & \cdots & 0 & 0 & 0 & 0 \\
0 & 0 & \mathbf{\Phi}_1(x_{\mathrm{r}1}) & -\mathbf{I}_{12} & 0 & 0 & \cdots & 0 & 0 & 0 & 0 \\
0 & 0 & 0 & 0 & \mathbf{\Phi}_{\mathrm{h}1}(x_{\mathrm{l}1}) & -\mathbf{I}_6 & \cdots & 0 & 0 & 0 & 0 \\
\vdots & \vdots & \vdots & \vdots & \vdots & \vdots & \ddots & \vdots & \vdots & \vdots & \vdots \\
0 & 0 & 0 & 0 & 0 & 0 & 0 & \mathbf{\Phi}_N(x_{\mathrm{r}N}) & -\mathbf{I}_{12} & 0 & 0 \\
0 & 0 & 0 & 0 & 0 & 0 & \cdots & 0 & 0 & \mathbf{\Phi}_{\mathrm{h}N+1}(x_{\mathrm{r}N}) & -\mathbf{I}_6 \\
0 & 0 & -\mathbf{I}_6 & \mathbf{G} & 0 & 0 & \cdots & 0 & 0 & 0 & 0 \\
0 & 0 & 0 & 0 & \mathbf{G} & -\mathbf{I}_6 & \cdots & 0 & 0 & 0 & 0 \\
\vdots & \vdots & \vdots & \vdots & \vdots & \vdots & \ddots & \vdots & \vdots & \vdots & \vdots \\
0 & 0 & 0 & 0 & 0 & 0 & \cdots & \mathbf{G} & 0 & 0 & 0 \\
0 & 0 & 0 & 0 & 0 & 0 & \cdots & 0 & \mathbf{G} & -\mathbf{I}_6 & 0 \\
0 & 0 & \mathbf{D}_{\mathrm{l}1} & \mathbf{D}_{\mathrm{r}1} & 0 & 0 & \cdots & 0 & 0 & 0 & 0 \\
\vdots & \vdots & \vdots & \vdots & \vdots & \vdots & \ddots & \vdots & \vdots & \vdots & \vdots \\
0 & 0 & 0 & 0 & 0 & 0 & 0 & \mathbf{D}_{\mathrm{l}N} & \mathbf{D}_{\mathrm{r}N} & 0 & 0 \\
\mathbf{D}_{\mathrm{l}} & 0 & 0 & 0 & 0 & 0 & \cdots & 0 & 0 & 0 & \mathbf{D}_{\mathrm{r}}
\end{bmatrix},$$

$$\overline{\mathbf{d}} = \begin{bmatrix}
0 \\ 0 \\ 0 \\ \vdots \\ 0 \\ 0 \\ 0 \\ 0 \\ \vdots \\ 0 \\ 0 \\ \mathbf{d}_1 \\ \vdots \\ \mathbf{d}_N \\ \mathbf{d}_{\mathrm{h}}
\end{bmatrix} \tag{36}$$

$$\bar{\mathbf{y}} = \left[\mathbf{y}_{\mathrm{h}1}(0), \mathbf{y}_{\mathrm{h}1}(x_{\mathrm{l}1}), \mathbf{y}_1(x_{\mathrm{l}1}), \mathbf{y}_1(x_{\mathrm{r}1}), \mathbf{y}_{\mathrm{h}2}(x_{\mathrm{r}1}), \ldots, \mathbf{y}_N(x_{\mathrm{l}N}), \mathbf{y}_N(x_{\mathrm{r}N}), \mathbf{y}_{\mathrm{h}N+1}(x_{\mathrm{r}N}), \mathbf{y}_{\mathrm{h}N+1}(l)\right]^{\mathrm{T}}$$

For simple boundary cases of the host beam, $\mathbf{d}_h = 0$. Noting $\mathbf{d}_i$ in the boundary conditions of the actuator patches in Eq. (29), vector $\overline{\mathbf{d}}$ in Eq. (36) can be written as

$$\overline{\mathbf{d}} = \mathbf{\Psi}\bar{\mathbf{I}}_{\mathrm{op}} \tag{37}$$

where $\mathbf{\Psi}$ is a $(36N + 12) \times N$ photo-elastic coupling matrix, and

$$\bar{\mathbf{I}}_{\mathrm{op}} = (bp_{331}h_1 I_1^{\beta}, bp_{332}h_2 I_2^{\beta}, \ldots, bp_{33N}h_N I_N^{\beta})^{\mathrm{T}} \tag{38}$$

is the generalized light intensity vector. It should be noted that this generalized light intensity vector consists of nonlinear functions of the light intensity $\mathbf{I}_i$.

The state vectors at all interfaces can be obtained by

$$\bar{\mathbf{y}} = \overline{\mathbf{\Phi}\mathbf{I}}_{\mathrm{op}} \tag{39}$$

in which $\overline{\mathbf{\Phi}} = \mathbf{\Phi}^{-1}\mathbf{\Psi}$. Then the displacements and forces at any points can be obtained from Eqs. (26) and (27).

4. Wireless remote shape control

In static structural shape control, the objective is to find the light intensities that can actuate the structure to a shape that best matches the desired one. To do this, we need to employ the relationship between the light intensity applied onto the photo-actuators and the response of the composite beam, which has been established in the previous section. In this section, we divide the beam into many limited number of segments to develop the discrete equations. Using the procedure for Eq. (35), the general form of the discrete governing equation can be expressed as follows:

$$\mathbf{K}\mathbf{y} = \widetilde{\mathbf{\Psi}}\bar{\mathbf{I}}_{\mathrm{op}} \tag{40}$$

where $\mathbf{K} \in R^{n\times n}$ is the coefficient matrix, n is the total number of degree of freedom, $\mathbf{y} \in R^n$ is the state vector comprising of all forces and displacements, $\widetilde{\mathbf{\Psi}} \in R^{n\times N}$ is a coefficient matrix, and $\bar{\mathbf{I}}_{\mathrm{op}} \in R^N$ is the generalized light intensity vector. Since the light intensities are unknown in structural shape control problems, it is convenient to rewrite Eq. (40) in terms of light intensity vector $\mathbf{I}_{\mathrm{op}} = (I_1, I_2, \ldots, I_N)$. Let us consider a more general discrete governing equation given by

$$\mathbf{K}\mathbf{y} = \mathbf{g}_{\mathrm{op}}(\mathbf{I}_{\mathrm{op}}) \tag{41}$$

$\mathbf{g}_{\mathrm{op}} \in R^n$ is the vector that is a nonlinear function of the intensity vector $\mathbf{I}_{\mathrm{op}} = (I_1, I_2, \ldots, I_N)^{\mathrm{T}}$.

To control the shape of the host beam, we need to extract the displacements and forces of the host beam from the state vector. In addition, we also need to pick up the interested displacements or generalized forces from the state vector of the host beam and set weighting factors to them. In doing so, we consider a generalized "shape" defined by

$$\mathbf{s} = \mathbf{R}\mathbf{y} \tag{42}$$

where $\mathbf{R} \in R^{m\times n}$ is a weighting matrix, and $\mathbf{s} \in R^m$ is an index vector, which can be either longitudinal displacement, axial force, transverse displacement, rotational angle, transverse shear force and bending moment or their combination depending on the selection of the weighting matrix.

In structural shape control, the control inputs to the actuators are obtained by minimizing a defined error function between the actuated and the desired shapes. For a given desired shape $\mathbf{s}_{\mathrm{d}} \in R^m$, we define the error function as

$$e = (\mathbf{s} - \mathbf{s}_{\mathrm{d}})^{\mathrm{T}}(\mathbf{s} - \mathbf{s}_{\mathrm{d}}) = |\mathbf{s} - \mathbf{s}_{\mathrm{d}}|^2 \tag{43}$$

Solving $\mathbf{y}$ from Eq. (41) and substituting it to Eqs. (42) and (43), we have

$$e(\mathbf{I}_{\mathrm{op}}) = \mathbf{g}^{\mathrm{T}}(\mathbf{I}_{\mathrm{op}})\mathbf{H}\mathbf{g}(\mathbf{I}_{\mathrm{op}}) - 2\mathbf{b}^{\mathrm{T}}\mathbf{g}(\mathbf{I}_{\mathrm{op}}) + \mathbf{s}_{\mathrm{d}}^{\mathrm{T}}\mathbf{s}_{\mathrm{d}} \tag{44}$$

where

$$\mathbf{H} = \mathbf{K}^{-\mathrm{T}}\mathbf{R}^{\mathrm{T}}\mathbf{R}\mathbf{K}^{-1} \in R^{n\times n}; \quad \mathbf{b} = \mathbf{K}^{-\mathrm{T}}\mathbf{R}^{\mathrm{T}}\mathbf{s}_{\mathrm{d}} \in R^n \tag{45}$$

To find the control light intensities applied to photo-actuators that minimizes the square difference e, the first order differentiation of the error function e with respect to $\mathbf{I}_{\mathrm{op}}$ should be zero, and this yields the following equation:

$$\mathbf{g}^{\mathrm{T}}(\mathbf{I}_{\mathrm{op}})\mathbf{H}\frac{\partial \mathbf{g}(\mathbf{I}_{\mathrm{op}})}{\partial \mathbf{I}_{\mathrm{op}}} + \mathbf{b}^{\mathrm{T}}\frac{\partial \mathbf{g}(\mathbf{I}_{\mathrm{op}})}{\partial \mathbf{I}_{\mathrm{op}}} = 0 \tag{46}$$

where $\frac{\partial \mathbf{g}(\mathbf{I}_{\mathrm{op}})}{\partial \mathbf{I}_{\mathrm{op}}} \in R^{n\times N}$ is the Jacobian matrix.

The nonlinear algebraic equations in Eq. (46) can be solved by an iterative procedure. Employing Taylor series expansion and neglecting the nonlinear terms, the control force $\mathbf{g}(\mathbf{I}_{\mathrm{op}})$ can be expanded approximately as

$$\mathbf{g}(\mathbf{I}_{\mathrm{op}j+1}) \approx \mathbf{g}(\mathbf{I}_{\mathrm{op}j}) + \frac{\partial \mathbf{g}(\mathbf{I}_{\mathrm{op}j})}{\partial \mathbf{I}_{\mathrm{op}}}(\mathbf{I}_{\mathrm{op}j+1} - \mathbf{I}_{\mathrm{op}j}); \quad \frac{\partial \mathbf{g}(\mathbf{I}_{\mathrm{op}j+1})}{\partial \mathbf{I}_{\mathrm{op}}} \approx \frac{\partial \mathbf{g}(\mathbf{I}_{\mathrm{op}j})}{\partial \mathbf{I}_{\mathrm{op}}} \tag{47}$$

Substituting Eq (47) into (46), the following iterative procedure can be obtained:

$$\mathbf{I}_{\mathrm{op}j+1} = \mathbf{I}_{\mathrm{op}j} - [\mathbf{J}^{\mathrm{T}}(\mathbf{I}_{\mathrm{op}j})\mathbf{H}\mathbf{J}(\mathbf{I}_{op_i})]^{-1}\mathbf{J}^{\mathrm{T}}(\mathbf{H}\mathbf{g}(\mathbf{I}_{\mathrm{op}j}) + \mathbf{b}) \tag{48}$$

The optimal light intensity can be the determined using the iteration procedure developed in Eq. (48).

5. Simulation examples

The host beam in the simulations is a cantilever aluminium beam with geometrical dimensions of 110 mm × 5 mm × 0.8 mm and Young's modulus of 70 GPa. The photostrictive actuators are made of PLZT (3/52/48) ceramics which comprises a 3 at.% lanthanum substitution into a 52 at.% lead zirconate 48% lead titanate solid solution. The actuator patch is cut into the sizes of 5 mm × 5 mm and polished to a thickness of 1 mm. Its two side surfaces are coated with Ag to form a pair of electrodes, and it is polarized in the direction from one electrode to the other one. The Young's modulus of the PLZT is 68 GPa, and its piezoelectric strain constant is 320×10^{-12} m/V. It has been found in experiment that the photovoltage of this material is proportional to the square root of light intensity (Poosanaas et al., 2000), i.e.,

$$E_{\mathrm{ph}} = p_{33} I_{\mathrm{op}}^{0.5} \tag{49}$$

The photostrictive constant for this actuator patch is taken as $p_{33} = 0.66$ V/(mW)$^{0.5}$ = 20.87 V/W$^{0.5}$.

5.1. Beam responses with fixed light intensity

Firstly, the response of a beam with illumination intensity will be examined. A single photostrictive actuator is bonded on the host beam. The distance between the left edge of this actuator and the fixed end of the beam is 5 mm. The adhesive layer has a thickness of 0.05 mm, and its Young's modulus and Poisson's ratio are 3 GPa and 0.4, respectively. When the actuator is irradiated by near ultraviolet light with a light intensity of 4000 W/m^2 (400 mW/cm^2), the displacements and forces at any point of the beam are determined from Eqs. (39), (32) and (33). The displacements and force results of the beam are given in Fig. 4. It can be seen from Fig. 4 that the longitudinal displacement in the actuator patch is much larger than that in the associated segment of the host beam. Whereas the transverse displacement and the rotation angle in the actuator patch are very close to those in the corresponding segment of the host beam. The axial force and the shear force in the actuator patch have the same magnitudes as those in the relevant segment of the host beam but have opposite signs to balance with each other. The tip deflection of the host beam is 0.143 μm when the small photostrictive actuator is irradiated by near ultraviolet light with a light intensity of 400 mW/cm^2. Using more actuator patches, a larger tip deflection of the host beam can be achieved.

The transverse displacement at the free end of the host beam actuated by the actuator with different light intensities is depicted in Fig. 5. As shown in Fig. 5, the tip deflection of the host beam increases as the light intensity becomes strong. The relationship between the tip deflection and light intensity is nonlinear.

5.2. Optimum light intensity distribution for desired structure shape

We will perform static shape control of the cantilever beam using more photostrictive actuator patches. Consider that ten identical photostrictive patches are bonded to one of the surfaces of the cantilever beam as the actuators and gap between any two adjacent actuators is 5 mm. The left edge of the first actuator is 5 mm away from the fixed end and the right side of the last actuator is 10 mm away from the free end of the host beam. The desired shape of the host beam is described by the follow function:

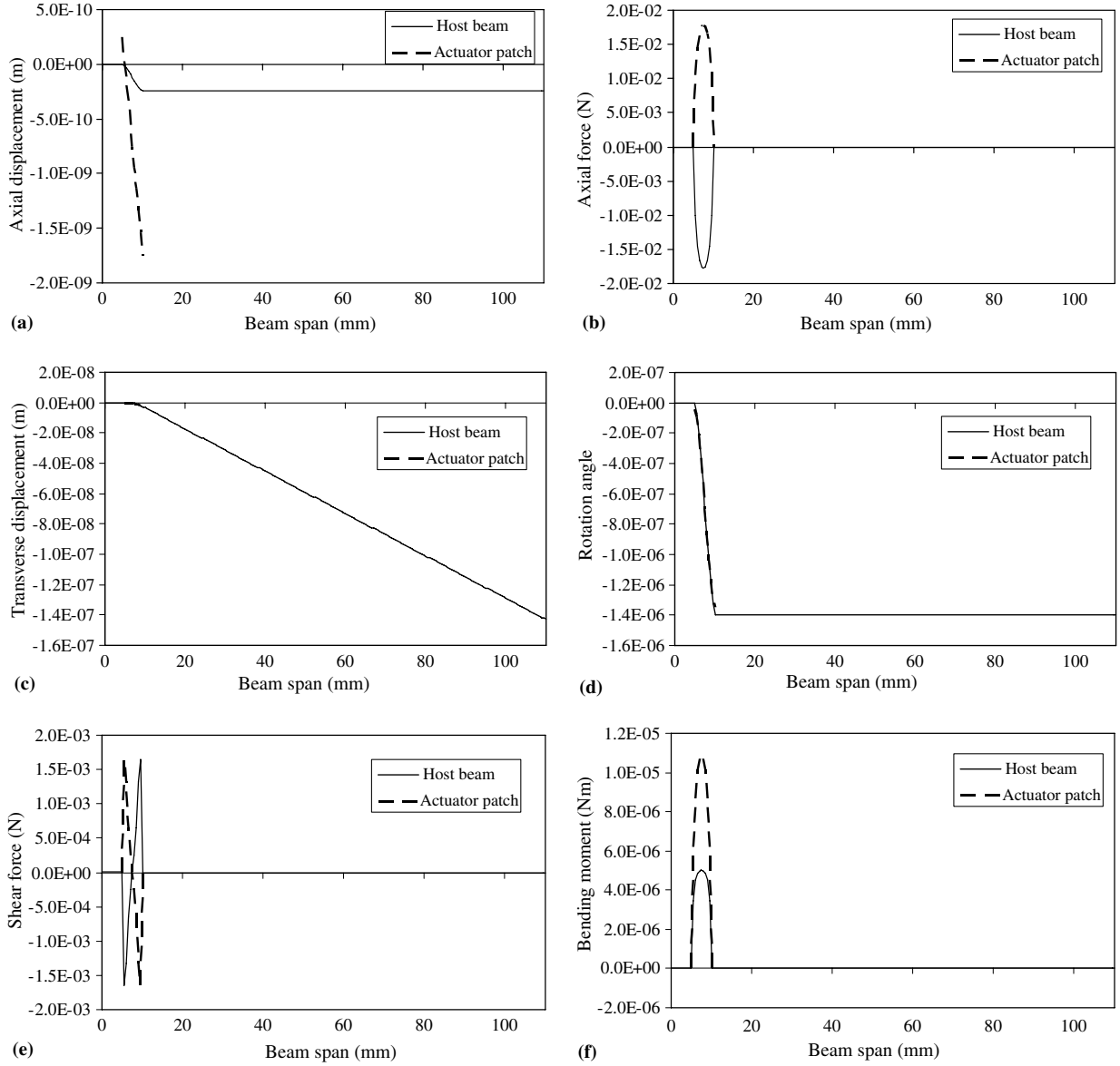

Fig. 4. Displacements and forces induced by the photostrictive actuator. (a) Longitudinal displacement, (b) axial force, (c) transverse displacement, (d) rotation angle, (e) transverse shear force and (f) bending moment.

$$w_{\mathrm{d}}(x) = A_{\mathrm{d}}\left[\cos\left(\frac{\pi x}{3l}\right) - 1\right]$$

where $A_{\mathrm{d}} = 1 \times 10^{-6}$ m. To achieve a shape that best match the desired shape, the optimal control light intensities for all actuators are calculated using the procedure described in the previous section. These light intensities are 4113, 663, 1901, 1396, 1390, 1229, 1071, 969, 616 and 1052 W/m^2, respectively. The polling directions of all these actuators are along the same direction. The actuated shape of the host beam by these optimal light intensities is depicted in Fig. 6, in which the desired shape is also plotted for comparison. This figure shows that the actuated shape matches well with the desired one, and the square error between them is 1.13×10^{-17}.

Consider another desired shape with one stationary node defined by

$$w_{\mathrm{d}}(x) = 3 \times 10^{-7}\left[\cos\left(\frac{\pi x}{3l}\right) - 1\right]\sin\left(\frac{5\pi x}{4l}\right)$$

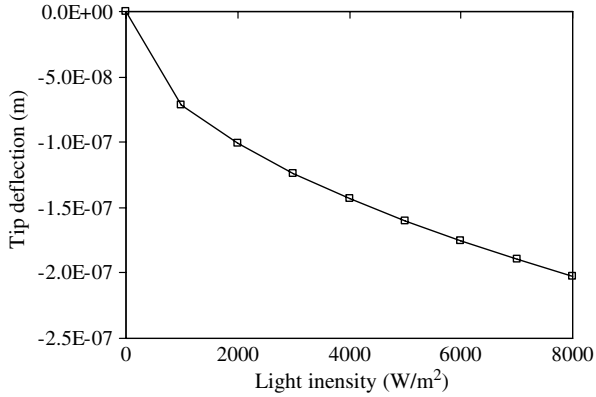

Fig. 5. Tip deflection versus light intensity.

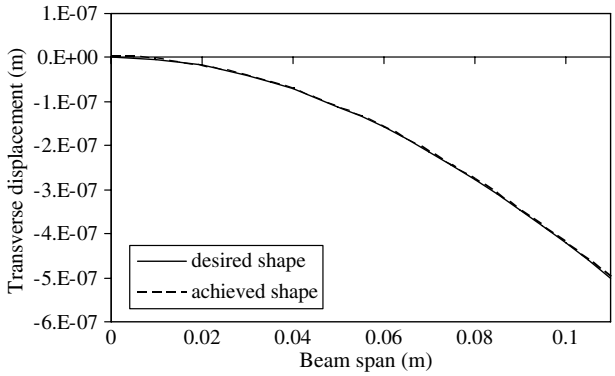

Fig. 6. The desired and actuated beam shapes.

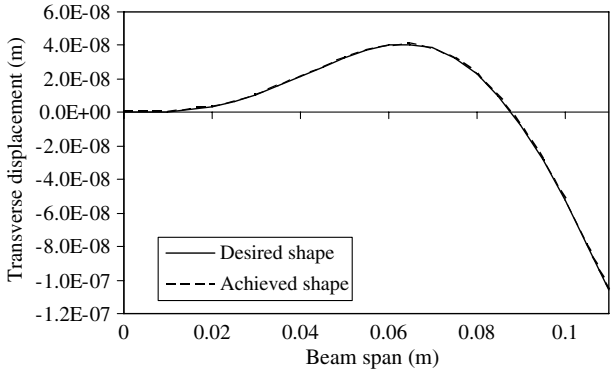

Fig. 7. Desired and actuated beam shapes with one node.

the obtained optimal light intensities for the actuators are 105, 300, 331, 60, 130, 1258, 3282, 5115, 4299, 3308 W/m^2, respectively. In this case, however, the polling directions of the first four actuators close to the left end of the beam are opposite to those of the rest six actuators. The actuated shape by the optimal light intensities together with the desired shapes is depicted in Fig. 7. The square error for this case is also very small which indicates that the desired shape is achieved by the photostrictive actuators with optimized light intensities irradiated on them.

6. Conclusions

This paper explores the applications of the novel photostrictive materials in wireless remote control of flexible structures. After a brief review of the constitutive relationships between the induced strain and the light intensity irradiated on the photostrictive materials, the interaction between photo-induced strain/stress in the actuators and the deformation of the host structures bonded with those actuators are investigated. A nonlinear model of a beam with several photostrictive actuators is established and governing equations derived. The analytical solution for the governing equations is given in terms of transitions matrices segment by segment. Based on this model, an iterative procedure for static structural shape control of beams using nonlinear photostrictive actuators is given. Simulation examples show that a single small photostrictive actuator is capable of actuating a thin beam. A given desired shape of beam can be achieved using several photostrictive actuators under optimal light intensities, which are in a reasonable range of light power.

Acknowledgements

The authors are grateful to the support of the Australian Research Council via Discovery-Projects Grants (Grant Nos. DP0210716 and DP0346419).

References

Baglio, S., Castorina, S., Fortuna, L., et al., 2002. Modeling and design of novel photo-thermo-mechanical microactuators. Sensors and Actuators A – Physical 101 (1–2), 185–193.

Belforte, G., Eula, G., Ferraresi, C., et al., 1998. Mechanical microactuators with photostrictive control. JSME International Journal Series C – Mechanical Systems Machine Elements and Manufacturing 41 (4), 886–892.

Cho, Y.W., Choi, S.K., Vysochanskii, Y.M., 2001. Photovoltaic effect of Sn2P2S6 ferroelectric crystal and ceramics. Journal of Materials Research 16 (11), 3317–3322.

Dalba, G., Doubovik, E., Fridkin, V.M., et al., 1996. The circular bulk photovoltaic effect in the piezoelectric crystal La3Ga5SiO14:Pr. Ferroelectrics Letters 21 (3–4), 61–63.

Fridkin, V.M., 1979. Photoferroelectrics. Springer, New York.

Fridkin, V.M., Lasarev, V.G., Levin, J.E., et al., 1984. The influence of the magnetic-field on the bulk photovoltaic effect in the piezoelectric ZNS. Ferroelectrics Letters 2 (2), 97–100.

Fridkin, V.M., Lazarev, V.G., Shlenski, A.L., et al., 1987. The influence of the magnetic-field on the circular bulk photovoltaic current in the piezoelectric BI12GEO20. Ferroelectrics 73 (3–4), 379–382.

Fukuda, T., Hattori, S., Arai, F., Nakamura, H., 1995. Performance improvement of optical actuator by double side irradiation. IEEE Transactions on Industrial Electronics 42 (5), 455–461.

Goldring, D., Zalevsky, Z., Goldenberg, E., et al., 2003. Optical characteristics of the compound PLZT. Applied Optics 42 (32), 6536–6543.

Ichiki, M., Morikawa, Y., Mabune, Y., et al., 2004. Preparation and photo-induced properties of lead lanthanum zirconate titanate multilayers. Journal of Physics, D: Applied Physics 37, 3017–3024.

Kawaguchi, K., Ichiki, M., Morikawa, Y., Nakada, T., 2002. Electrical properties of photovoltaic PLZT and its application to optical motors. Ferroelectrics 273, 41–46.

Kittel, C., 1996. Introduction to Solid States Physics, seventh ed. John Wiley and Sons, Inc., New York.

Lin, C.T., Li, L., Mcneill, J.D., et al., 1994. Photoconductivity of extrinsic ion-doped PLZT ceramics. Journal of Luminescence 60 (1), 170–174.

Liu, B., Tzou, H.S., 1998. Distributed photostrictive actuation and opto-piezothermoelasticity applied to vibration control of plates. Journal of Vibration and Acoustics 120, 937–943.

Morikawa, Y., Nakada, T., 1998. Bimorph-type optical actuator using PLZT elements – (position control of optical actuator by on-off control). JSME International Journal Series C – Mechanical Systems Machine Elements and Manufacturing 41 (4), 860–866.

Nonaka, K., Akiyama, M., Hagio, T., et al., 1998. Photostriction in lead lanthanum zirconate titanate ceramics enhanced by the additive effect. Journal of the Ceramic Society of Japan 106 (7), 641–644.

Uchino, K., 1997. New applications of photostrictive ferroics. Materials Research Innovations 1 (3), 163–168.

Poosanaas, P., Tonooka, K., Uchino, P., 2000. Photostrictive actuators. Mechatronics 10, 467–487.

Zhou, L.J., Zimmermann, A., Zeng, Y.P., et al., 2004. Effects of PbO content on the sintering behavior, microstructure, and properties of La-doped PZST antiferroelectric ceramics. Journal of Materials Science – Materials in Electronics 15 (3), 145–151.

Tzou, H.S., Chou, C.S., 1996. Nonlinear opto-electromechanics and photodeformation of optical actuators. Smart Materials and Structures. 5, 230–235.